Nuclear Instruments and Methods in Physics Research B 323 (2014) 1–6

Contents lists available at ScienceDirect

Nuclear Instruments and Methods in Physics Research B

journal homepage: www.elsevier.com/locate/nimb

An investigation on the removal characteristics of compound materials during ion beam sputtering using the Kinetic Monte Carlo method

Xiao Liang [a], Xiang Wang [a,*], Erlong Miao [b], Jinjin Zheng [a], Fei Wang [b], Gaowen Wang [b], Yongqiang Gu [b]

[a] Department of Precision Machinery and Precision Instrumentation, University of Science and Technology of China, Hefei, Anhui 230026, PR China
[b] Changchun Institute of Optics, Fine Mechanics and Physics, Chinese Academy of Sciences, Changchun, Jilin 130033, PR China

ARTICLE INFO

Article history:
Received 30 October 2013
Received in revised form 10 January 2014
Available online 1 February 2014

Keywords:
Ion beam
Binary compound
Removal characteristics
Preferential sputtering
Kinetic Monte Carlo simulation

ABSTRACT

Ion beam sputtering has been extensively adopted for optical surface processing. Due to differences between atoms in terms of atomic mass, surface binding energy and surface coverage fraction, the removal characteristics of the solid compound materials will be diverse. This paper first developed a quasi-atomistic model of the binary compound target and simulated ion beam sputtering processes using the Kinetic Monte Carlo (KMC) method. Furthermore, the effect of atomic differences on the removal characteristics was investigated. Finally, contrastive analysis between simulations and experiments of fused silica using an Ar^+ ion beam was performed. The simulation results indicated that the competition between two types of preferential sputtering could cause the surface composition, removal amount and removal rate to oscillate in the early stage and to be relatively stable after a period of time. Compared with the fused silica experiments, the stable removal rate error of the KMC model considering the preferential sputtering is 5.9%; however, the stable removal rate error of the KMC model without regard to the preferential sputtering is 12.6%.

1. Introduction

Ion beam sputtering is a physical process in which energetic ions bombard a solid surface and then remove surface atoms. Relying on its atomic-scale removal capacity and non-contacting mode, ion beam sputtering has been widely adopted to for the fabrication of high-precision optical components [1,2] and the acquirement of the ultra-smooth surface used in X-ray systems and deep/extreme ultraviolet lithography [3,4], the production of ion-induced periodic surface patterns [5,6], and manufacturing of nano- and micro-engineering structures if the beam is controllably focused [7,8].

The basic theory of sputtering removal of material was classically developed by Sigmund [9]. Stoyanov et al. [10] and Adams and Vasile [11] have presented mathematical modeling and experimental studies on the accurate control over the removal amount of elementary substances by applying Sigmund's formula of sputtering yield. Hartmann et al. [12] also used Sigmund's theory to build their Monte Carlo models for the sputtering procedure of an elementary substance in their simulation studies on the formation of ion-induced surface patterns.

The principal ingredient of SiO_2, CaF_2, SiC, etc. materials that are pervasively applied to optical elements is the compound rather than the elementary substance. Atoms of different elements have different weights, surface binding energies, surface coverage fractions (which refer to the coverage fraction of each type of atom on the surface), etc. These different physical properties, affecting the interaction between impinging ions and material atoms, cause atoms of different elements to have different removal characteristics, such as removal amounts and removal rates. The effects of the atomic mass and binding energy on the sputtering yield of compounds have been reported by various scientists [14–16], and Kudryavtsev [17] conducted a general mathematical derivation of the effects of the surface and bulk concentration of different components on the sputtering yield of multicomponent targets. Concurrently, the Monte Carlo (MC) method is widely employed as a random sampling and statistical method in simulating various transport phenomena of particles and non-deterministic physical problems. By virtue of the stochastic mechanism between the ion beam and solid material atoms, this method is already in use in ion beam sputtering simulation studies [12,13,18–20].

On this basis, to understand the differences of removal characteristics in compound materials sputtered by ions, the Kinetic Monte Carlo (KMC) method based on Sigmund's theory is utilized to computationally model the ion beam sputtering procedure of binary compound materials in this article. Distinctions between atoms of different elements are incarnated from three perspec-

* Corresponding author. Tel.: +86 0551 63601484.
E-mail addresses: xiao@mail.ustc.edu.cn (X. Liang), wxyf@ustc.edu.cn (X. Wang), miaoel@sklao.ac.cn (E. Miao), jjzheng@ustc.edu.cn (J. Zheng), wangf@sklao.ac.cn (F. Wang), wanggw@sklao.ac.cn (G. Wang), yqgu82@gmail.com (Y. Gu).

0168-583X/$ - see front matter © 2014 Elsevier B.V. All rights reserved.
http://dx.doi.org/10.1016/j.nimb.2014.01.010

tives, including the atomic mass, surface binding energy and surface coverage. Afterwards, we simulate, analyze and discuss the removal characteristics, such as the removal amount and removal rate, on a three-dimensional substrate model. Finally, this report provides a contrastive analysis with the sputtering experiment in which an Ar^+ ion beam bombards the fused silica surface.

2. Methodology

2.1. Expressions of duality

For ion beam sputtering, the near-surface sputtering behavior is affected by the properties of the incident ions, type and distribution of target atoms. Under the aforementioned sputtering theory [9], the surface atom's energy normal to the surface, derived from cascades, must be greater than the surface binding energy (SBE) when it attempts to escape the target. Thus, atoms of smaller SBE can be sputtered more easily. Likewise, a lighter atom can obtain more kinetic energy from cascades; hence, atoms of smaller mass will have a greater chance to be removed. This phenomenon that atoms with different masses and SBEs possess different probabilities to be sputtered is called preferential sputtering [14,21,22], which we call the intrinsic preferential effect (IPE) because of the inherency of atomic mass and SBE. Due to intrinsic preferential sputtering, the easier-sputtered atoms (smaller mass and SBE) are given priority to be eroded. Therefore, the surface coverage of the harder-sputtered atoms (larger mass and SBE) will increase. Then, the percentage of the cascade energy received by harder-sputtered atoms will increase, and these atoms will obtain more opportunities to be sputtered off. We call this type of preferential sputtering depending on the surface coverage the coverage preferential effect (CPE). Given the above, sputtering on the surface of a binary compound A_xB_y is not only affected by the atomic mass M_i (i = A, B) and the surface binding energy U_i but also the sputtering time t and the time-varying surface coverage $S_i(t)$. Thus, during the ion beam removal processes, the "removal" has different characteristics due to atomic differences.

2.2. Calculation model for ion sputtering

To achieve a quasi-atomistic Monte Carlo strategy, the geometric model of the binary compound material A_xB_y is as follows: A cube of size 'LD' represents an atom, and a solid-on-solid cubic lattice is adopted as the material substrate, as illustrated in Fig. 1. Two types of atoms are distributed randomly at a certain percentage. The surface is defined as a time-dependent height function $H(x,y,t)$, $(1 \leqslant x \leqslant L, 1 \leqslant y \leqslant L)$. At time t_i, if a surface atom at position (x_i,y_i) is removed, the height at this position is expressed by $(H(x_i,y_i,t_i) - 1)$. Therefore, the removal amount unit area can be represented by the variation of the surface average height $\overline{H(t)}$, namely, $V_{KMC}(t_i) = \overline{H(t_i)} - \overline{H(t_{i-1})}$. $\overline{H(t)}$ can be described as

$$\overline{H(t)} = \frac{1}{Ns}\sum_{x,y\in\omega} H(x,y,t), \tag{1}$$

where ω is the partial surface region affected by incoming ions, and Ns is the quantity of surface-atoms in this region.

For the Kinetic Monte Carlo modeling of the ion beam sputtering process, we set the removal procedure as mainly a series of ion sputtering events. Suppose that the number of events initiated by one certain ion is N, and these N events constitute the "Event Table (ET)" of this ion. The probability $P_i(i = 1,2,...,N)$ of one event being selected depends on its share of the whole ET [22]. The execution of each event corresponds to one certain surface atom being removed. After that, the quantity and distribution of surface atoms changes, and the surface topography evolves. Notice that the ET is updated with every incoming ion.

In Sigmund's sputtering theory, the material removal rate somewhere on the surface depends on the deposited energy from the incident ions, which release their energy with a Gaussian distribution [9]. As illustrated in Fig. 2, an ion with energy E and an oblique angle θ bombards the surface at the point O' and penetrates along the incidence direction, i.e., the positive Z' axis in the local coordinate system O'–$X'Y'Z'$. At point O, as the energy scattering center with a depth $d(E)$, its kinetic energy E is given according to a Gaussian distribution that has a parallel width $\sigma(E)$ and a perpendicular width $\mu(E)$ to the incident trajectory. The deposited energy captured by the surface atom i (A or B) at position (x',y',z') is ΔE_i. If $\Delta E_i > U_i$, then atom i can be sputtered off, and the probability is proportional to ΔE_i:

$$\Delta E_i = \frac{E}{(\sqrt{2\pi})^3\sigma(E)\mu(E)^2}\exp\left\{-\frac{[z'-d(E)]^2}{2\sigma(E)^2} - \frac{x'^2+y'^2}{2\mu(E)^2}\right\}. \tag{2}$$

Hence, we can use the normalized energy deposition distribution as the probability distribution of sputtering a single surface atom:

$$P_i = \frac{S_i(t)\cdot f_i\cdot \Delta E_i}{\sum_i^N (S_i(t)\cdot f_i\cdot \Delta E_i)}, \tag{3}$$

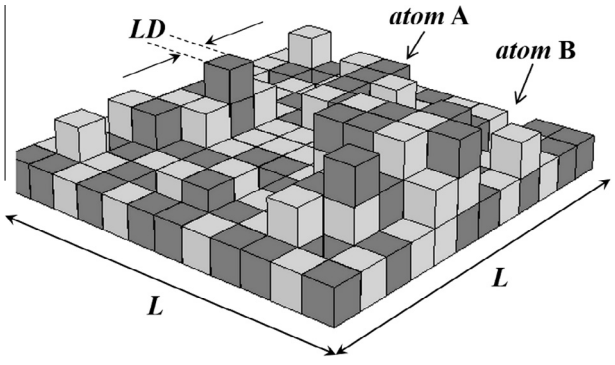

Fig. 1. The geometric model of the compound material consisting of two types of atoms: A (represented by dark gray cubes) and B (represented by light gray cubes).

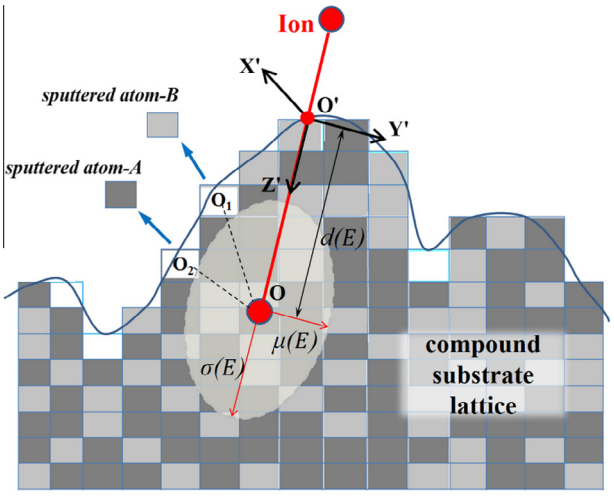

Fig. 2. Schematic of the energy distribution of the incident ion and the induced sputtering behaviors (e.g., A or B atom at site O_1 or O_2) as described in our article. The red line segment stands for the incoming trajectory. (For interpretation of the references to color in this figure legend, the reader is referred to the web version of this article.)

where $S_i(t)$ is the surface coverage fraction and represents the aforementioned CPE. f_i is the preferential factor and represents the IPE:

$$f_i = M_i^{-2m} \cdot U_i^{2m-1}. \quad (4)$$

A larger f_i indicates that the IPE is more significant. m is a constant related to the ion energy, and its value could be taken to be 0.25 for low-energy ion sputtering (e.g., 600–1200 eV) [14]. When m is certain, the penetration distance $d(E) \propto E^{2m}$ [14]; hence,

$$d(E) = d_0 \cdot (E/E_0)^{1/2}. \quad (5)$$

During low-energy ion beam sputtering, the relationship between the penetration distance and the energy distribution width is given as $d(E) = 2\sigma(E) = 2.5\mu(E)$ because of the property that $d(E)/\sigma(E)$ and $d(E)/\mu(E)$ do not change with E [23].

2.3. Model of beam characteristics

We regard the continuous ion beam as a series of ion packs, each of which is composed of a controllable number of ions possessing the same E and θ. Every ion pack includes a total of C_0 ions, and the dwell time of one pack is set to one second. For the Gaussian beam, the average ion flux of a suite of packs with a diameter D is $\varphi = C_0/[\pi(D/2)^2]$ $ions \cdot atom^{-1} \cdot s^{-1}$, and the density distribution satisfies a Gaussian density function $g(x) = (1/\sqrt{2\pi}\sigma_b)$ $\exp(-x^2/2\sigma_b^2)$ with $FWHM = 0.707\,D$, where x is the distance between the ion and the center axis of the pack and $x \in [0,D/2]$. Therefore, the material removal characteristics can be determined from the sampling of incident ions, the calculation for the energy received by surface atoms and the occurrence probabilities of sputtering events, the execution of specific events, and statistics on a series of ion packs. The main steps are as follows:

1) *Ion sampling*: Set the ions of one ion-pack to the same ion energy and the same incident angle. Select one incident ion and its location via sampling according to the Gaussian density function $g(x)$.
2) *Building the Event Table*: The selected ion is incident to the target model. Use Eq. (2) to calculate the energy (ΔE_i) received by each surface atom and record the atoms that satisfy $\Delta E_i > U_i$ as independent events in the event table (ET). Therefore, we can determine all the atoms that can be sputtered.
3) *Sputtering event sampling*: Use Eq. (3) to calculate the occurrence probability of every event in the ET, and use random numbers to sample the probabilities. Thus, we can determine the quantities and locations of these selected "sputtered atoms."
4) *Topography statistics*: If an atom at position (x_i,y_i) on the surface is judged to be "sputtered", perform the operation $(H(x_i,y_i,t_i) - 1)$. Then, go to Step 1 and determine another ion via sampling $g(x)$. When all the ions of one ion pack have been selected, run statistics on the execution results of all the selected events. Thus, we can obtain an updated surface/topography for every ion pack.

3. Results and discussion

3.1. Simulation of ion beam sputtering

We started the KMC program to simulate and calculate the ion beam sputtering procedure on a 5000 $LD \times 5000$ LD binary substrate model, for which the initial rms roughness was set to 2.5 LD rms and the peak-to-valley difference value varied in the range of [0, 50 LD]. The oblique angle θ with respect to the surface normal was 0°, and the sputtering time t was 0–80 s. The solid material referenced the fused silica used widely in optical elements; hence, target atoms were divided into Si-type (A) and O-type (B). Corresponding material parameters and beam parameters relevant to the KMC calculation are listed in Table 1. We can determine that the average ion flux in KMC processes is $\varphi_{KMC} \approx 3.06$ $ions \cdot atom^{-1} \cdot s^{-1}$.The calculation results based on a 5000 LD $\times$ 5000 LD surface are displayed in Fig. 3. The left column (a and d) shows the initial surface without sputtering (i.e., $t = 0$). The middle column (b and e) and right column (c and f) show the surface topography and the curve fitted from the central contour of the removal pit after sputtering processes of 30 and 60 ion packs, respectively. Thus, it can be observed that the depth of the removal pit increases with the sputtering time (i.e., the quantity of ion packs), and the removal amount unit area is calculated as $V_{KMC}(30s) = 161.3$ LD and $V_{KMC}(60s) = 309.8$ LD. Furthermore, from the two curves fitted by the central contour of two removal pits, we can obtain Gaussian removal functions with $FWHM_{30s} = 2784$ LD and $FWHM_{60s} = 2679$ LD, respectively.

3.2. Discussion on removal characteristics

According to Eq. (1), the surface average height $\overline{H(t)}$ with time is presented in Fig. 4a and the surface removal rate $R_{surf}(t)$ $(= d\overline{H(t)}/dt)$ representing the removed thickness unit time is presented in Fig. 4b. In terms of the two images, $\overline{H(t)}$ descends wavily and $R_{surf}(t)$ oscillates clearly before $t = 25$ s. Additionally, 25 s later, $\overline{H(t)}$ gradually enters a linear decrease, and $R_{surf}(t)$ stabilizes around 4.95 LD/s.

Based on Table 1, both the mass and SBE of the B-atom are smaller than those of the A-atom; hence, $f_A \approx 0.0878 < f_B \approx 0.1550$ between the preferential factors of A and B based on the description in Section 2.1 and Eq. (4). It is easy to see that B-atoms should belong to easier-eroded atoms (EEA) and that A-atoms should belong to harder-eroded atoms (HEA). When B-atoms are removed more rapidly because of higher IPE, the surface coverage of A-atoms $S_A(t)$ changes as illustrated in Fig. 5. At the beginning stage, $S_A(t)$ increases from 33.33% to over 50% rapidly, and such an ascent of the surface coverage will enhance the CPE of A-atoms. Then, this reinforcing bias toward HEA on the surface distribution will boost the removal rate of HEA (i.e., A-atoms here), and $S_A(t)$ begins to decline. However, when $S_A(t)$ decreases to some extent, the intrinsic preferential effect (IPE, $f_A < f_B$) will accelerate the removal processes of B-atoms again. Via such repeated ups and downs, $S_A(t)$ can finally reach a relatively stable state. As shown in Fig. 5, the surface coverage of A-atoms stabilizes at 46.15 ± 2.50% after an oscillating process of approximately 25 s, which differs from the initial 33.33%. It follows that the competition between IPE and CPE of EEA and HEA results in an oscillating surface coverage initially and eventually maintains the surface coverage of HEA at a higher level than the initial state.

3.3. Experiments and comparisons

A series of experiments were performed in this article for comparisons with our simulation results. A Kaufman-type Ar^+ ion beam

Table 1
Material parameters and KMC calculation parameters in single ion-pack sputtering.

Material parameters			KMC parameters	
A atom (Si)	M_A	28	E_0	600 eV
	U_A	4.63	d_0	10 LD
	$S_A(0)$	33.3%	σ_0	5 LD
B atom (O)	M_B	16	μ_0	4 LD
	U_B	2.6	C_0	6×10^7
	$S_B(0)$	66.7%	D	5000 LD

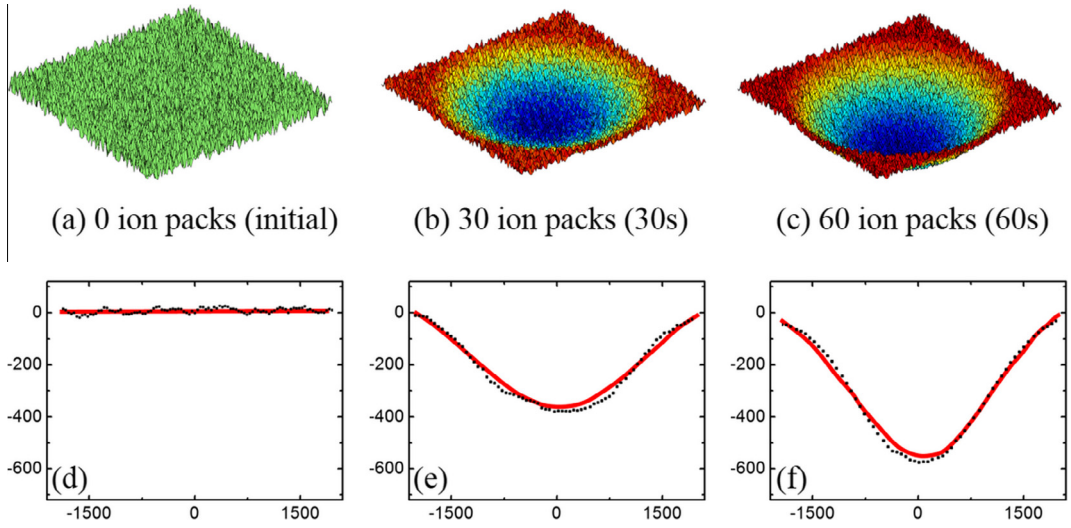

Fig. 3. Simulation images showing the 5000 *LD* × 5000 *LD*-sized surface during KMC ion beam sputtering. The upper row represents the oblique view of the surface with the sputtering time = (a) 0, (b) 30 and (c) 60 ion packs. The lower row illustrates the shape of the removal pit, measured in *LD*, at sputtering time of (d) 0, (e) 30 and (f) 60 ion packs. Inside, the red lines indicate the fitted central contour of the removal pit. (For interpretation of the references to color in this figure legend, the reader is referred to the web version of this article.)

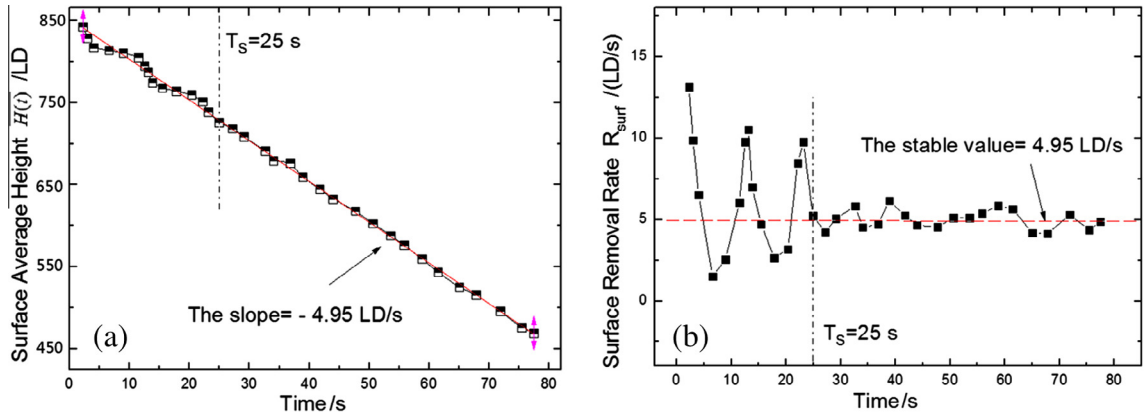

Fig. 4. The time dependence of (a) the surface average height representing the removal amount, measured in *LD*, and (b) the surface removal rate, measured in *LD*/s. The variate T_S denotes the critical time transferring from the oscillating stage to the relatively stable stage.

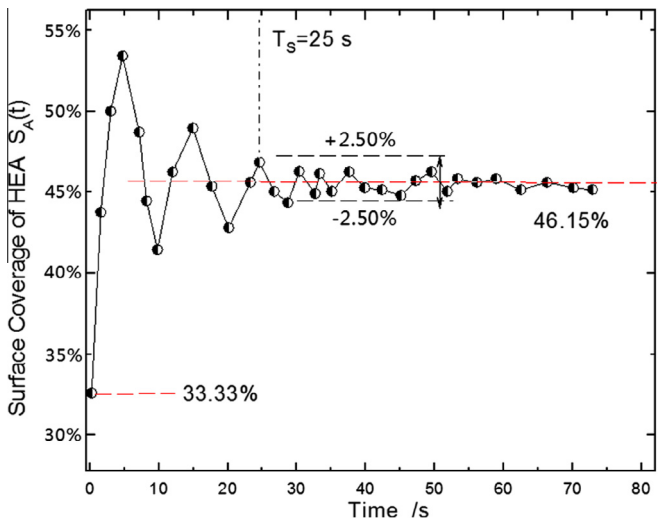

Fig. 5. The time dependence of the surface coverage of harder-eroded atoms (i.e., A-atoms here), measured in 100% and seconds. The variate T_S denotes the critical time transferring from the oscillating stage to the relatively stable stage.

with the energy of 600–1200 eV and the flux Φ of approximately 3×10^{15} *atoms* · $cm^{-2} \cdot s^{-1}$ was applied vertically onto the fused silica surface with an initial roughness of approximately 0.87 nm *rms*. The surface atomic density η of fused silica $\approx 10^{15}$ *atoms* · cm^{-2}; therefore, the average ion flux φ_{exp} in the experiments is $\varphi_{exp} = \Phi/\eta \approx 3$ *atoms* · $cm^{-2} \cdot s^{-1}$, nearly equal to φ_{KMC} in our KMC calculations.

The left column of Fig. 6a and c shows the unprocessed surface of the fused silica. The right column of Fig. 6b and d presents the measured removal results (via a Zygo GPI white-light interferometer with a wavelength of 632.8 nm) on a 1 × 1 mm surface region by Ar^+ ions when $E = 600$ eV and $t = 30$ s. The average removal amount unit area (i.e., the reduction of the average height $\overline{H(t)}$) is 53.8 nm, and the surface removal rate R_{surf} is 1.802 nm · s^{-1}. Through the fitted curve of the removal pit, we can also determine a Gaussian removal function with $FWHM_{30s} = 563.1$ μm, partly related to the KMC results in Fig. 3e and f.

To further probe the removal characteristics under different conditions, aiming at a binary solid material similar to fused silica, we utilized the KMC program to simulate removal processes and performed a comparative analysis with the experimental results. In addition, to evaluate the effect of preferential sputtering on

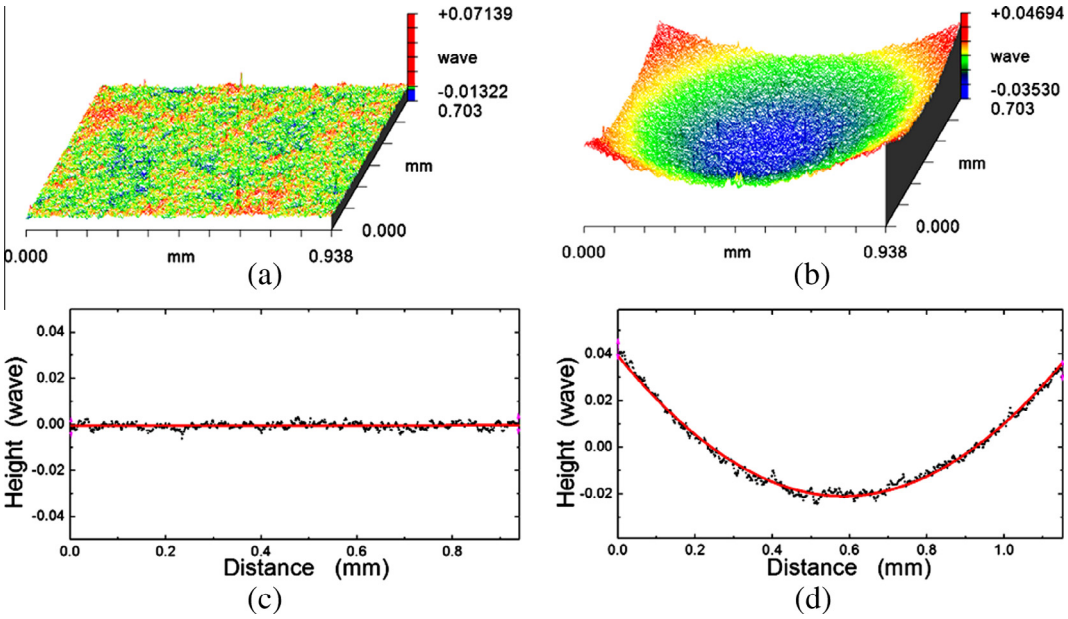

Fig. 6. White-light interferometer images showing the 1 × 1 mm surface of fused silica by Ar^+ ion beam sputtering. The upper row represents the oblique plot with the sputtering time of (a) 0 s and (b) 30 s. The lower row (c and d) illustrates the corresponding fitted central contour.

the surface removal characteristics, we established two different KMC computational models by the selection of the preferential factor f_i: a KMC model considering preferential sputtering (KMC_PS, herein $f_A \neq f_B$) and a KMC model without preferential sputtering (KMC_NO_PS, herein $f_A = f_B$). Based on these models, analysis and comparisons of removal characteristics were performed.

Fused silica is an amorphous form of silicon dioxide with long-range disorder and isotropy, and its interatomic distance mostly is 1.5–5.5 Å. Thus, the simulative cubic scale in our KMC calculation will approach the atomic scale of fused silica on the condition that 1 *LD* = 3.5, Å = 0.35 nm. In this case, the initial surface roughness 2.5 *LD rms* in KMC processes is 0.875 nm *rms*, which is approximately equal to the initial surface roughness of our fused silica sample (0.87 nm *rms*).

The selection of our KMC computational parameters all referred to experimental arguments based on fused silica, and there is consistency in the atom-scale and ion flux. Although the impact area of ions is in the range of μm, limited by the computation amount and the computation speed, while the impact area in experiments is in the range of mm, the surface removal rate changes little with the increasing simulation size based on our calculations under different-sized conditions. Therefore, we can utilize the removal rate to perform a comparative analysis between the simulation and experimental results.

In this paper, by orthogonally designing the experiment and simulation, we have acquired three types of results for different time and energy levels: the experimental result (EXP), the KMC result considering preferential sputtering (KMC_PS) and the KMC result without preferential sputtering (KMC_NO_PS). Features of the surface removal rate for the three states are presented in Fig. 7.

Fig. 7a shows the surface removal rate R_{EXP} from ion beam experiments for $t = 30$, 45, 60, 75 s and $E = 600$, 800, 1000, 1200 eV. Fig. 7b and c shows the surface removal rate R_{KMC} from the KMC_PS model and the KMC_NO_PS model, respectively, for $t = 30$–75 s and $E = 600$–1200 eV. The color distributions in Fig. 7d and e express the distributions of the relative deviation δ_R of the KMC_PS rate in 7b and the KMC_NO_PS rate in 7c from the experimental rate R_{EXP} in 7a, that is:

$$\delta_R = |(R_{KMC} - R_{EXP}^{In})/R_{KMC}|, \tag{6}$$

where R_{EXP}^{In} is the interpolated R_{EXP}. Note that the color, not the vertical ordinate, denotes the deviation δ_R in Fig. 7d and e.

A comparison among Fig. 7a–c reveals that R_{EXP} and R_{KMC} primarily follow the same trend: the surface removal rate remains almost unchanged with the changing dwell time but increases with increasing ion energy. According to the phenomena reflected by Figs. 4b and 5, after a period, the removal rate would remain stable

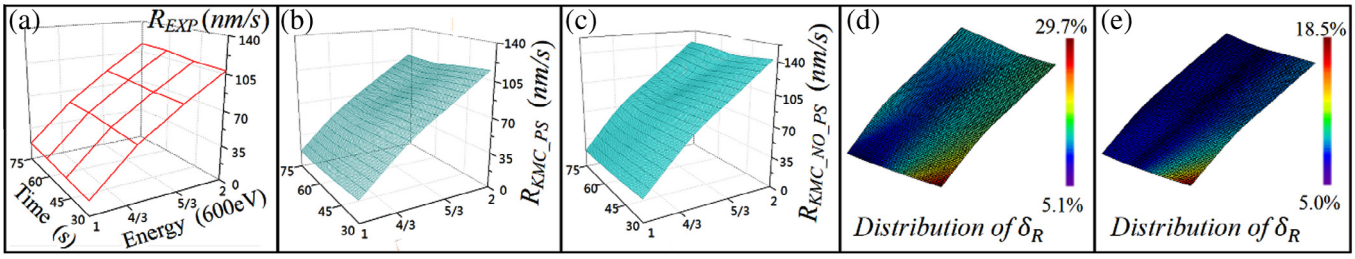

Fig. 7. Plots of the surface removal rate from three types of results for different time levels and different energy levels: (a) data measured from ion beam experiments under the conditions that the time is 30, 45, 60 and 75 s and the energy is 600, 800, 1000 and 1200 eV; (b) data calculated from the KMC_PS model within the time of 30–75 s and the energy of 600–1200 eV; (c) data calculated from the KMC_NO_PS model within the same conditions as (b). Additionally, the color distributions in (d) and (e) express separately the relative deviation distributions of data in (b) and (c) from data in (a).

at a certain level rather than oscillate with time. Therefore, the revealed trend of R_{EXP} and R_{KMC} corresponds with this conclusion.

The relative deviation of the KMC_PS result from the experimental result δ'_R is 5.0–18.5% (Fig. 7d), and the average deviation is 5.9%. The relative deviation of the KMC_NO_PS result from the experimental result δ''_R is 5.1–29.7% (Fig. 7e), and the average deviation is 12.6%. The main causes for δ_R is that our KMC removal computation did not contain surface diffusion behaviors, which affect the surface coverage of the binary material (i.e., affect the CPE) and then affect the surface removal rate. A magnitude difference exists between the experimental area and the simulation area due to restrictions of the computation amount and the computation speed, which affects on the results and could be another source of error. In addition, the assumption of certain simulation parameters, such as $[d_0\ \sigma_0\ \mu_0]$ in Table 1, could cause the deviation of the simulative sputtering yield (the average quantity of atoms removed per incident ion) from the real sputtering yield, resulting in the deviation of the surface removal rate from the real value.

However, we can see from Fig. 7d and e that relative to the KMC_NO_PS simulation, the calculation result of the KMC_PS model exhibits smaller deviations from the experimental results. In addition, the vital role that the preferential sputtering effect plays in the ion beam sputtering of binary materials it demonstrated.

4. Conclusions

This paper has utilized the Kinetic Monte Carlo method to model the ion beam sputtering procedure in terms of atomic mass, surface binding energy and surface coverage, and has studied removal characteristics such as the variation of surface coverage, the average removal amount and the removal rate of compound materials in combination with experiments of fused silica using an Ar^+ ion beam. The following conclusions have been drawn:

(1) The competition between the intrinsic preferential effect and the coverage preferential effect of harder-eroded-atoms and easier-eroded-atoms causes an oscillating variation in the surface composition, the average removal amount, and the removal rate during the early sputtering stage and eventually results in a relatively stable state.
(2) Under different conditions of dwell time and ion energy, the removal rate calculated by either the KMC model considering preferential sputtering (KMC_PS) or the KMC model without preferential sputtering (KMC_NO_PS) follows the same trend as the experimental removal rate determined for a fused silica surface using an Ar^+ ion beam: the surface removal is almost independent of the dwell time (after 30 s), but increases with increasing ion energy.
(3) Compared with the KMC_NO_PS simulation, the KMC_PS model possesses higher precision with respect to the experimental results and can better reflect the actual surface sputtering processes during ion beam machining.

Although this study has elucidated some instructive consequences by adding the preferential effect of the ion beam treating the binary compound material to our Kinetic Monte Carlo computational model, the absence of a surface diffusion mechanism, re-deposition mechanism, secondary sputtering, etc. causes our simulation to have a certain error. Therefore, adding more atomic mechanisms to the KMC model to further understand the various surface evolutions during ion beam sputtering would be an interesting investigation.

Acknowledgments

The authors are grateful to NSFC-CAS Joint Fund (No. U1332130), 111 Projects (No. B07033), 973 Project (No. 2014CB931804), and the State Key Laboratory of Applied Optics (PR China) for financial support of this study. We would also like to thank Huaijiang Yang, Yongxin Sui and Zhanlong Ma for very useful experimental guidance and technical support with the ion beam machining systems and materials.

References

[1] X. Xie, L. Zhou, Y. Dai, S. Li, Ion beam machining error control and correction for small scale optics, Appl. Opt. 50 (2011) 5221–5227.
[2] Y. Dai, W. Liao, L. Zhou, S. Chen, X. Xie, Ion beam figuring of high-slope surfaces based on figure error compensation algorithm, Appl. Opt. 49 (2010) 6630–6636.
[3] F. Frost, R. Fechner, B. Ziberi, J. Völlner, D. Flamm, A. Schindler, Large area smoothing of surfaces by ion bombardment: fundamentals and applications, J. Phys.: Condens. Matter 21 (2009) 224026.
[4] S. Mahmud, T. Fukabori, S. Pahlovy, I. Miyamoto, Low energy ion beam smoothening of artificially synthesized single crystal diamond chips with initial surface roughness of 0.08–0.4 nm rms, Diamond Relat. Mater. 24 (2012) 116–120.
[5] A. Keller, S. Facsko, W. Möller, Evolution of ion-induced ripple patterns on SiO_2 surfaces, Nucl. Instrum. Methods Phys. Res., Sect. B 267 (2009) 656–659.
[6] J. Vollner, B. Ziberi, F. Frost, B. Rauschenbach, Topography evolution mechanism on fused silica during low-energy ion beam sputtering, J. Appl.Phys. 109 (2011) 043501.1–043501.6.
[7] D. Allen, P. Shore, R. Evans, C. Fanara, W. O'Brien, S. Marson, W. O'Neill, Ion beam, focused ion beam, and plasma discharge machining, CIRP Ann.-Manuf. Technol. 58 (2009) 647–662.
[8] Y. Drezner, Y. Greenzweig, A. Raveh, Strategy for focused ion beam compound material removal for circuit editing, J. Vac. Sci. Technol., B: Microelectron. Nanometer Struct. 30 (2012) 011207.1–011207.9.
[9] P. Sigmund, Theory of sputtering. I. Sputtering yield of amorphous and polycrystalline targets, Phys. Rev. 184 (1969) 383.
[10] S. Stoyanov, C. Bailey, Y. Tang, S. Marson, A. Dyer, D. Allen, M. Desmulliez, Computational modelling and optimisation of the fabrication of nanostructures using focused ion beam and imprint forming technologies, Journal of Physics: Conference Series, IOP Publishing, 2010, pp. 012008.
[11] D. Adams, M. Vasile, Accurate focused ion beam sculpting of silicon using a variable pixel dwell time approach, J. Vac. Sci. Technol., B: Microelectron. Nanometer Struct. 24 (2006) 836–844.
[12] A.K. Hartmann, R. Kree, U. Geyer, M. Kölbel, Long-time effects in a simulation model of sputter erosion, Phys. Rev. B 65 (2002) 193403.
[13] Y. Tan, Y. Song, P. Zhou, C. Wang, H. Yang, Monte Carlo simulation for the sputtering yield of Si3N4 thin film milled by focused ion beams, Optoelectron. Lett. 4 (2008) 273–275.
[14] R. Behrisch, Sputtering by particle bombardment I. Physical sputtering of single-element solids, vol. 47, Springer, Berlin, 1981.
[15] P. Sigmund, Fundamental processes in sputtering of atoms and molecules (SPUT92): symposium on the occasion of the 250th anniversary of the Royal Danish Academy of Sciences and Letters, Copenhagen, 30 August-4 September, 1992: invited reviews, Kongelige Danske Videnskabernes Selskab.43, 1 (1993).
[16] J. Malherbe, Sputtering of compound semiconductor surfaces. I: Ion–solid interactions and sputtering yields, Crit. Rev. Solid State Mater. Sci. 19 (1994) 55–127.
[17] Y. Kudryavtsev, Ion beam sputtering of multicomponent targets: surface composition change and cluster emission, Tech. Phys. 57 (2012) 247–250.
[18] E. Chason, W. Chan, M. Bharathi, Kinetic Monte Carlo simulations of ion-induced ripple formation: dependence on flux, temperature, and defect concentration in the linear regime, Phys. Rev. B 74 (2006) 224103.
[19] C. Borschel, C. Ronning, Ion beam irradiation of nanostructures – A 3D Monte Carlo simulation code, Nucl. Instrum. Methods Phys. Res., Sect. B 269 (2011) 2133–2138.
[20] R. Kree, T. Yasseri, A. Hartmann, The influence of beam divergence on ion-beam induced surface patterns, Nucl. Instrum. Methods Phys. Res., Sect. B 267 (2009) 1407–1411.
[21] M. Seah, T. Nunney, Sputtering yields of compounds using argon ions, J. Phys. D Appl. Phys. 43 (2010) 253001.
[22] J.B. Adams, Z. Wang, Y. Li, Modeling Cu thin film growth, Thin Solid Films 365 (2000) 201–210.
[23] M.A. Makeev, R. Cuerno, A.-L. Barabási, Morphology of ion-sputtered surfaces, Nucl. Instrum. Methods Phys. Res., Sect. B 197 (2002) 185–227.